Author/s:
Kim, C-J;Gu, Y;Xu, W;Shin, S;Mazaheri, O;Quinn, JF;Caruso, F

Title:
Supramolecular Assembly of Charge-Tunable Metal–Phenolic Networks

Date:
2025

Citation:
Kim, C. -J., Gu, Y., Xu, W., Shin, S., Mazaheri, O., Quinn, J. F. & Caruso, F. (2025). Supramolecular Assembly of Charge-Tunable Metal–Phenolic Networks. Chemistry of Materials, 37 (2), pp.676-686. https://doi.org/10.1021/acs.chemmater.4c02617.

Persistent Link:
https://hdl.handle.net/11343/354928

Supramolecular Assembly of Charge-Tunable Metal–Phenolic Networks

Chan-Jin Kim,[†,‡] Yuang Gu,[†] Wanjun Xu,[†] Subin Shin,[†] Omid Mazaheri,[†] John F. Quinn,[£,#] and Frank Caruso[,†]*

[†]Department of Chemical Engineering, The University of Melbourne, Parkville, Victoria 3010, Australia

[‡]Department of Chemical Engineering, Gyeongsang National University, Jinju 52828, Republic of Korea

[£]Drug Delivery, Disposition and Dynamics Theme, Monash Institute of Pharmaceutical Sciences, Monash University, Parkville, Victoria 3052, Australia

[#]Department of Chemical Engineering, Faculty of Engineering, Monash University, Clayton, Victoria 3800, Australia

*Corresponding author. Email: fcaruso@unimelb.edu.au (F.C.)

ABSTRACT

Controlling the surface charge of nano-assembled structures enables modulation of their physicochemical properties and expands their applications. Metal–phenolic networks (MPNs) typically yield materials with negatively charged surfaces. Herein, MPNs with tunable surface charge were prepared using biscatechol-functionalized poly(2-vinylpyridine) (P2VP) and various metal ions. The first assembly route yielded P2VP–Fe^{III} MPN capsules that displayed pH-dependent surface charge reversal (~ −10 mV at pH 12 to 20 mV at pH 2) and facilitated the

fabrication of hollow superstructures. Besides the catechol–metal interaction, the pyridinyl nitrogen–metal coordination facilitated the continuous growth of P2VP–Co^{II} MPN capsules (e.g., 12–26 nm over 24 h). The second assembly route involving concurrent quaternization of P2VP and MPN assembly produced positively charged capsules (i.e., QP2VP/P2VP–Fe^{III} MPN capsules) and provided control of the shell thickness (12–52 nm) and surface charge (6–53 mV) over time (1–8 h) at 70 °C. The positively charged surfaces enabled the fabrication of bioactive and fluorescent capsules and regulation of the cell association properties depending on the degree of positive charge. This work expands the selection of negatively or positively charged MPN building blocks for designing tunable MPN systems.

INTRODUCTION

Extensive progress in the fabrication of functional materials has been made through using functional supramolecular building blocks ranging from small molecules (e.g., peptides and polyphenols) to macromolecules (e.g., polymers and oligonucleotides).[1–4] Supramolecular assemblies are built upon the interplay of various noncovalent interactions between building blocks such as metal coordination, hydrogen bonding, and π–π, ionic, and hydrophobic interactions.[5–7] These assemblies have been employed in materials science and biomedical applications, including particle engineering,[8,9] therapeutic delivery,[10,11] catalysis,[12,13] biological imaging,[5,14] and energy storage.[15]

Metal–phenolic networks (MPNs) are emerging metal–organic supramolecular assemblies constructed from metal ions and phenolic molecules.[16] These supramolecular networks have advanced coating technologies, enabling tailor-made optimization of the properties of particle systems, and have been extensively exploited owing to their simple, robust, and modular synthesis procedures. The selection of phenolic building blocks, such as natural phenolics (e.g., tannic acid,

epigallocatechin gallate, gallic acid, and pyrocatechol) and phenolic-functionalized polymers (e.g., 2-, 4-, 8-arm poly(ethylene glycol)), influences the physicochemical properties of the resulting MPN assemblies; these properties include permeability, shell thickness, and cell association.[17,18] In addition, stimuli-responsive building blocks, such as quercetin, poly(*N*-isopropylacrylamide), and DNA block copolymers, have been used to fabricate functional MPN systems with guest-responsiveness,[19] thermoresponsiveness,[9] and programmability.[20] However, the surface charge of most MPN assemblies is generally negative owing to the intrinsic properties of phenolic molecules and metal–phenolic complexation.[21] Endowing MPNs with tunable surface charge is expected to expand the range of MPN materials and expand their application scope.

To address tuning of the surface charge of MPN, herein we examine phenolic ligand-conjugated polymers as alternative MPN building blocks. Poly(vinylpyridine)s (PVPs), including the isomers poly(2-vinylpyridine) (P2VP) and poly(4-vinylpyridine), are polymer chains that have a similar chemical structure to polystyrene but with a nitrogen atom in the aromatic ring (i.e., pyridine).[22,23] The pyridinyl nitrogen in PVP confers versatile physicochemical properties. (1) The hydrophilicity and charge of PVP chains are dependent on pH owing to the basicity of the pyridine ring (pK_a of pyridinium ion = 5.23),[24] thus these polymer chains become water-soluble and positively charged under acidic conditions.[22] (2) PVPs can bind with metal ions and inorganic nanoparticles (NPs) upon coordination to the pyridinyl nitrogen.[25,26] (3) PVP chains may be transformed to permanent polycations through quaternization with alkyl halides (e.g., methyl iodide), and the degree of quaternization can be controlled by varying the stoichiometry and reaction temperature and/or time.[23,27] Owing to its attributes, PVP has been applied in the fabrication of magnetic, electronic, catalytic, conductive, and cargo-releasing materials, as well as soft materials for optical applications.[22,23]

Herein, we report particle systems that incorporate pyridine-based polymer chains (i.e., P2VP) as MPN building blocks. To build coordination networks with metal ions, P2VP chains were functionalized to have a catechol group at each end of the chain to form biscatechol-P2VP (Figure 1a). Negatively charged MPN capsules were then obtained through coordination networks between biscatechol-P2VP and metal ions on a sacrificial template (Figure 1b, Assembly route 1 (A1)). In addition to catechol–metal coordination networks, these materials incorporate noncovalent interactions such as pyridinyl nitrogen–metal coordination, hydrogen bonding, and hydrophobic interactions between the building blocks. A pH-dependent surface charge reversal of the MPN capsules from negative to positive was realized upon deprotonation/protonation of the pyridine rings in the polymer blocks. Furthermore, secondary hollow superstructure formation and continuous growth of MPN films were achieved from the binding properties of pyridinyl nitrogen with inorganic NPs and metal ions. Using a different assembly route, positively charged MPN capsules were obtained by concurrent quaternization of pyridine groups by methyl iodide and MPN assembly (Figure 1b, A2). Electrostatic interactions between quaternized pyridine groups and catechol groups were involved in A2 in addition to the interactions occurring in A1 (Figure 1b). Furthermore, assembly route A2 enabled control of the shell thickness and surface charge of the MPN capsules by varying the assembly temperature and time and metal ion species. Harnessing the positively charged surface of the capsules, bioactive and fluorescent MPN capsules were prepared through the functionalization of the MPN capsules with negatively charged bioactive and fluorescent molecules (e.g., horseradish peroxidase (HRP) and fluorescein isothiocyanate-tagged dextran (FITC-dextran)). Moreover, the most positively charged MPN capsules showed a high loading amount (i.e., 340 mg g^{-1}) comparable to those achieved in mesoporous particles.[28] Likewise, the cell association properties of the MPN capsules with different surface charges could

be controlled. The present study demonstrates the important role of building blocks in expanding the library of MPNs in further broadening their potential application in materials science and biotechnology.

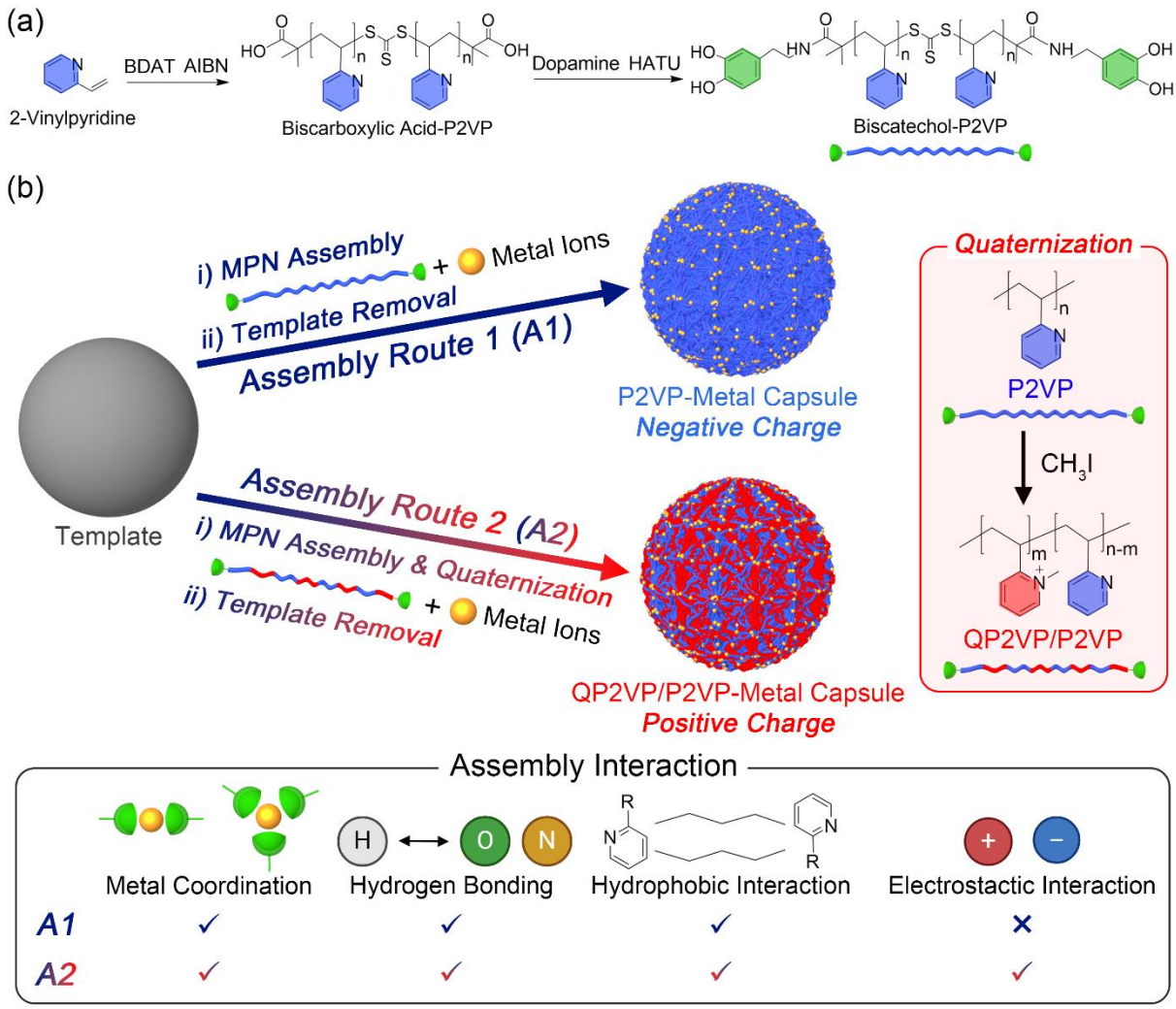

Figure 1. (a) Synthesis of biscatechol-functionalized P2VP (biscatechol-P2VP). (b) Schematic illustration of MPN assembly of P2VP–metal MPN capsules (negative charge) (assembly route 1, A1) and QP2VP/P2VP–metal MPN capsules (positive charge) (A2). The noncovalent interactions involved in A1 and A2 are depicted. AIBN, 2,2′-azobis(2-methylpropionitrile); HATU, hexafluorophosphate azabenzotriazole tetramethyl uronium.

EXPERIMENTAL SECTION

Synthesis of P2VP–Metal MPN Capsules. A carboxylic acid-functionalized polystyrene (PS-COOH) template particle dispersion (1.86 ± 0.03 μm, 100 mg mL^{-1}) (50 μL) was transferred to a 1.7 mL microcentrifuge tube containing ethanol (450 μL). The PS-COOH particles were washed twice with ethanol by vortexing and sonication for 1–2 min and then pelleted by centrifugation (2000*g*, 2 min). The supernatant was then discarded and the process was repeated. A biscatechol-polymer stock solution and $FeCl_3 \cdot 6H_2O$ solution were prepared in ethanol. These solutions were added to the PS-COOH particle suspension after which ethanol (380 μL) was added to obtain final concentrations of 10 mg mL^{-1} PS-COOH particles, 1.0 mM for P2VP, and 2 mM for metal ions (i.e., Fe^{III}, Al^{III}, V^{III}, Cr^{III}, or Co^{II}), with vortexing for 2 min. The catechol/metal ion ratio was maintained at 1:1. To achieve continuous MPN film growth onto the PS-COOH particles, the mixtures were kept for the desired time under shaking at 1200 rpm. Excess and unreacted materials were then removed by pelleting the particles (2000*g*, 2 min) and the supernatant was discarded. The P2VP–metal MPN-coated particles were washed three times with ethanol (500 μL) by repeated centrifugation (2000*g*, 2 min) and redispersion. The particles were then resuspended in ethanol (50 μL) and kept in tetrahydrofuran (THF) (1 mL) overnight to remove the template particles. The resulting P2VP–metal MPN capsules were pelleted through centrifugation (2000*g*, 2 min) and washed with THF (500 μL) five times. At the final THF washing step, the capsules were pelleted through centrifugation (2000*g*, 3 min) and the supernatant was discarded. The P2VP–metal MPN capsules were washed with ethanol once and resuspended in ethanol or water (500 μL).

Quaternization of P2VP Chains. Biscatechol-functionalized $P2VP_{76}$ solution was mixed with methyl iodide (3.1 μL) to reach final concentrations of 1 mM polymer and 100 mM methyl iodide

in 500 μL ethanol. The mixtures were kept at 70 °C and stirred at 1200 rpm for different times (e.g., 1, 2, 3, 4, 5, 6, and 8 h). Thereafter, the quaternized samples (i.e., QP2VP/P2VP) were dried under vacuum and stored at −20 °C for further use.

Synthesis of QP2VP/P2VP–Metal MPN Capsules through Quaternization–MPN Assembly. To synthesize QP2VP/P2VP–metal MPN capsules, PS-COOH template particles were incubated with P2VP and metal ions following the same protocol as that used for the synthesis of P2VP–metal MPN capsules. The final concentrations of PS-COOH particles, P2VP, and metal ions (i.e., Fe^{III}, Cr^{III}, and Co^{II}) were 10 mg mL^{-1}, 1 mM, and 2 mM in ethanol (500 μL), respectively. To that solution containing PS-COOH particles, P2VP, and metal ions, methyl iodide (3.1 μL) was added to achieve simultaneous quaternization/MPN assembly, and the mixture was kept at the desired temperature (i.e., 50, 60, or 70 °C) under shaking at 1200 rpm for 1–8 h. Then, the particle suspension was transferred to a 1.7 mL microcentrifuge tube. Excess and unreacted materials were removed by pelleting the particles (2000*g*, 2 min) and the supernatant was discarded. The QP2VP/P2VP–metal MPN-coated particles were washed three times with ethanol (500 μL) by repeated centrifugation (2000*g*, 2 min) and redispersion. The particles were then resuspended in ethanol (50 μL) and kept in THF (1 mL) overnight to remove the template particles. Then, the QP2VP/P2VP–metal MPN capsules were pelleted through centrifugation (2000*g*, 2 min) and washed with THF (500 μL) five times. At the final THF washing step, the capsules were pelleted through centrifugation (2000*g*, 3 min) and the supernatant was discarded. The P2VP–metal MPN capsules were washed with water twice and resuspended in water (500 μL).

Synthesis of Bioactive/Fluorescent MPN Capsules. Flow cytometry was used to count the number of QP2VP/P2VP–Fe^{III} MPN capsules, and the concentration of the capsules was set to 2 × 10^8 mL^{-1}. To synthesize bioactive MPN capsules, QP2VP/P2VP–Fe^{III} MPN capsules (0.25 mL,

2×10^8 mL^{-1}) were incubated with HRP solution (125 μL, 20 mg mL^{-1}) in 10 mM 3-(*N*-morpholino)propanesulfonic acid (MOPS) (pH 7) for 8 h under shaking at 1200 rpm. The HRP-loaded capsules were then washed with 10 mM MOPS (pH 7) (2000*g*, 2 min) twice to remove unbound HRP and then resuspended in 10 mM MOPS (pH 7) (500 μL). The loading amount was calculated by comparing the absorbances at 400 nm of the protein solution before loading and the supernatant after loading.

To fabricate fluorescent MPN capsules, QP2VP/P2VP–Fe^{III} MPN capsules (0.25 mL, 2×10^8 mL^{-1}) were incubated in 2000 kDa FITC-dextran at varying concentrations in water for 16 h under the shaking at 1200 rpm. The final concentrations of FITC-dextran were 1, 2, 3, 4, and 5 mg mL^{-1}. The FITC-dextran-loaded capsules were then washed with water (2000*g*, 2 min) twice to remove unbound FITC-dextran and then resuspended in water (500 μL).

RESULTS AND DISCUSSION

Synthesis of Versatile MPN Capsules. A biscarboxyl acid-terminated trithiocarbonate chain transfer agent, bis(α,α′-dimethyl-α″-acetic acid)-trithiocarbonate (BDAT), was synthesized and characterized by nuclear magnetic resonance (^{1}H NMR) spectroscopy (Figure S1).[29] Biscarboxylic acid-functionalized P2VP (biscarboxylic acid-P2VP) was synthesized by reversible addition–fragmentation chain transfer polymerization using BDAT as the chain transfer agent. Three polymers with different degrees of polymerization (*n*) were synthesized and characterized by NMR spectroscopy and gel permeation chromatography: biscarboxylic acid-$P2VP_{32}$ (number-average molecular weight (M_n) = 3600 g mol^{-1}, n = 32); biscarboxylic acid-$P2VP_{76}$ (M_n = 8300 g mol^{-1}, n = 76); and biscarboxylic acid-$P2VP_{128}$ (M_n = 13700 g mol^{-1}, n = 128) (Figures S2 and S3 and Table S1). Thereafter, biscatechol-P2VPs were synthesized through amide bond formation between the terminal carboxylic acid groups of the polymer chains and the amine group of

dopamine at a high dopamine/P2VP ratio (i.e., 10:1) (Figures 1a and S3).[8] Fourier transform infrared spectroscopy analysis showed the phenol O–H stretching band at 3400 cm^{-1} from the catechol groups in the $P2VP_{76}$ chain, indicating the successful synthesis of biscatechol-$P2VP_{76}$ (Figure S4).[30] The characteristic ligand-to-metal charge transfer band around 600 nm was detected for the biscatechol-$P2VP_{76}$–Fe^{III} system in ethanol, indicating bis- and tris-complex coordination between Fe^{III} ions and the catechol groups in the polymer chains (Figure S5).[16] In contrast, the ligand-to-metal charge transfer band was absent from the spectrum of the biscarboxylic acid-$P2VP_{76}$–Fe^{III} system in ethanol.

P2VP–Fe^{III} MPN films were assembled on the surface of sacrificial templates (i.e., 1.86 μm PS-COOH particles) through multiple noncovalent interactions between the building blocks such as metal coordination, hydrogen bonding, and hydrophobic interactions.[8,20] $P2VP_{76}$–Fe^{III} MPN capsules were obtained after template removal (Figure 1b, A1) and characterized by atomic force microscopy (AFM) (Figure 2a). Well-defined capsules with folds and creases were observed, as consistent with the characteristic properties of air-dried capsules. The shell thickness of the capsules was determined to be 12.1 nm from the minimum thickness value in AFM measurements. The shell thickness of the capsules was independent of the degree of polymerization of the polymer—all three $P2VP_X$–Fe^{III} MPN capsules featured a film thickness of ~12 nm (Figure S6). $P2VP_{76}$ chains were thus employed for further characterization and experiments. $P2VP_{76}$–Fe^{III} MPNs were stable in various solutions, likely owing to the multiple assembly interactions between the building blocks such as metal coordination (catechol–Fe^{III} ions), hydrogen bonding (mainly, pyridinyl nitrogen–hydrogen from –NH or catechol groups), and hydrophobic interactions (P2VP chains) (Figures 1b, 2b, and S7a). Furthermore, the catechol and pyridine groups become negatively and positively charged through deprotonation/protonation process; catechol is

deprotonated in alkaline condition (i.e. > pH 7)[31] and pyridine is protonated in acidic condition (i.e., < pH 5.3).[24] The size of the capsules decreased in hydrochloric acid (HCl) (by 21%) and increased in sodium hydroxide (NaOH) (by 18%), indicating that the deprotonation/protonation of the catechol groups are likely major factors influencing size change (Figure S7b).[8] The size increase observed in ethylenediaminetetraacetic acid (EDTA) (by 19%) was likely due to loosening of the metal coordination networks.[32] The oxidation of the catechol to quinone groups in the building blocks was likely hindered by the entanglement of polymer chains, resulting in the stability of $P2VP_{76}$–Fe^{III} MPNs in the alkaline solution (i.e., 0.5 M NaOH (pH 13.7)).[8,33] The surface charge of conventional MPNs, which are composed of naturally occurred phenolics, can be made negative (from neutral) upon coordination between catechols and metal ions (i.e., –OH and $–O^-$ from catechol or galloyl groups).[34] In the current work, the capsules showed pH-responsive charge reversal behavior (e.g., –9 mV at pH 12 and 19 mV at pH 2) owing to the protonation/deprotonation of pyridine and catechol groups, which induced a change in surface charge from negative to positive (i.e., –OH and $–O^-$ from catechol groups; N and NH^+ from pyridine groups) (Figure 2c).

P2VP chains are known to bind with inorganic NPs upon interaction between the pyridinyl nitrogen atoms and NP surfaces.[35] This property was exploited to evaluate the use of $P2VP_{76}$–Fe^{III} MPN capsules as building cores to form secondary superstructures. Gold NPs (AuNPs, 12.8 nm) were synthesized by the established citrate reduction method and characterized by UV–vis spectrophotometry and transmission electron microscopy (Figure S8).[36] We hypothesized that the exposed pyridinyl nitrogen on the surface of $P2VP_{76}$–Fe^{III} MPN capsules would enable binding with AuNPs to form a microscale superstructure. As observed in Figure 2d, hollow superstructures were obtained by incubating the capsules (core) with the AuNPs (satellite). The presence of a

higher number of AuNPs resulted in hollow superstructures coated with a denser layer of AuNPs on the capsule surface.

Conventional MPN assembly generally results in a film thickness of about 10 nm, regardless of the metal ion or phenolic ligand used, owing to the discrete film growth of MPNs (i.e., kinetic trapping and symmetry breaking at the interface in a short time (<1 min)).[16,37,38] In contrast, the present work exploits the co-existence of two different coordination chemistries in the assembled structure (i.e., catechol–metal and pyridine–metal interactions). The coordination network between pyridinyl nitrogen atoms and metal ions facilitates continuous film growth, as indicated by the time-dependent thickness growth of the film. The shell thickness of $P2VP_{76}$–Co^{II} MPN capsules increased from 12.3 to 16.5, 19.5, and 26.3 nm as the assembly time increased from 0 to 4, 8, and 24 h (Figure 2e). We note that the assembly time point at 0 h effectively corresponds to the assembly time at 2 min, which indicates rapid assembly occurring within a short time. The shell thickness of $P2VP_{76}$–Al^{III}, $P2VP_{76}$–V^{III}, $P2VP_{76}$–Cr^{III}, and $P2VP_{76}$–Fe^{III} MPN capsules increased by ~50, ~48, ~61, and ~30%, respectively, as assembly progressed from 0 to 24 h (Figure S9).

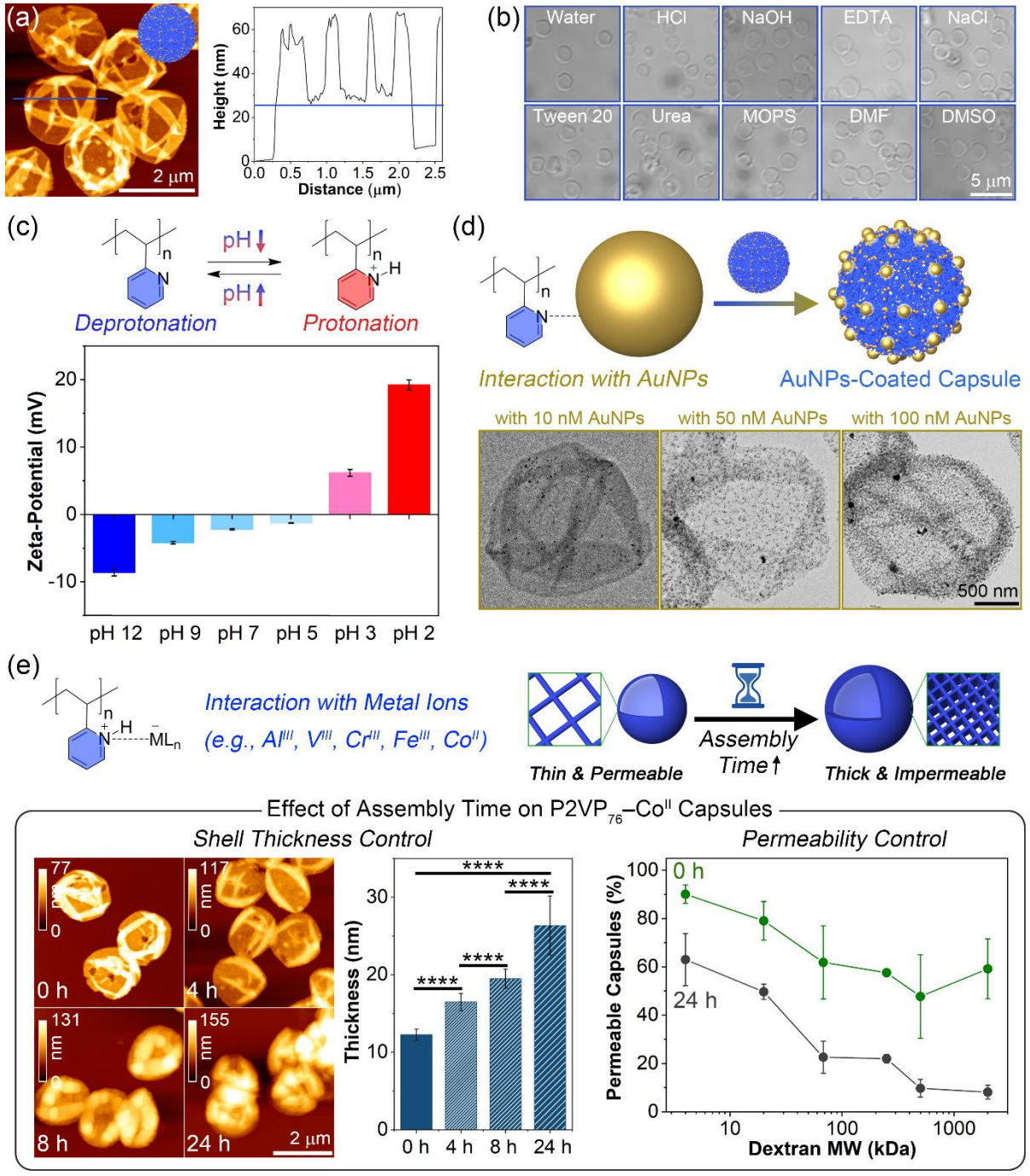

Figure 2. (a) Characterization of P2VP$_{76}$–Fe^{III} MPN capsules via AFM. The height–distance profile of an MPN capsule plotted along the blue line in the image is also shown. (b) Differential interference contrast images of P2VP$_{76}$–Fe^{III} MPN capsules in different solutions: water, HCl, NaOH, EDTA, sodium chloride (NaCl), Tween 20, urea, MOPS, dimethylformamide (DMF), and dimethyl sulfoxide (DMSO). (c) pH-Responsive surface charge reversal of P2VP$_{76}$–Fe^{III} MPN

capsules through the deprotonation/protonation of P2VP chains at different pHs. ζ-Potential values of $P2VP_{76}$–Fe^{III} MPN capsules in 10 mM NaOH (pH 12), 10 mM MOPS (pH 9, 7, 5, and 3), and 10 mM HCl (pH 2). (d) Preparation of a hollow superstructure composed of $P2VP_{76}$–Fe^{III} MPN capsule (core) and AuNPs (satellite) via the interaction between pyridine moieties in P2VP chains and AuNP surface. The ratios between MPN capsules and AuNPs (10, 50, and 100 nM) are 2.7×10^4, 13.3×10^4, 26.7×10^4, respectively. (e) Influence of assembly time on the properties (i.e., shell thickness and permeability) of $P2VP_{76}$–Co^{II} MPN capsules. The shell thickness of $P2VP_{76}$–Co^{II} MPN capsules prepared using different assembly times was determined by height–distance AFM analysis and is shown as the mean ± standard deviation of 10 independent AFM measurements. Statistical significance was determined by one-way analysis of variance (ANOVA): **** $p < 0.0001$. Permeability of $P2VP_{76}$–Co^{II} MPN capsules prepared using different assembly times (0 and 24 h) to FITC-dextran with M_w ranging from 4 to 2000 kDa. The permeability data are shown as the mean ± standard deviation of three independent experiments; 50–100 capsules were examined.

The permeability of capsules is influenced by the capsule shell thickness, with a thicker shell resulting in a reduced permeability.[8,17] The permeability of P2VP–metal MPN capsules prepared using different assembly times was determined by incubating the capsules with FITC-dextran molecules of M_w ranging from 4 to 2000 kDa (Figures 2e and S10). Capsules obtained after a longer assembly time were less permeable than those obtained after a shorter assembly time (Figures 2e and S10), indicating a higher degree of network entanglement in the thicker capsule shell. Specifically, as observed in Figure 2e, 59% and 8% of $P2VP_{76}$–Co^{II} capsules obtained after assembly times of 0 and 24 h, respectively, were permeable to 2000 kDa FITC-dextran. These findings demonstrate the use of P2VP as a versatile MPN building block in fabricating

multifunctional MPN capsules that feature pH-responsive charge reversal properties, hollow superstructure fabrication capability, and continuous film assembly capability.

Simultaneous Quaternization/MPN Assembly. Quaternization of PVP using alkyl halides imparts different physicochemical properties by providing permanent ionization (i.e., positive charge) to the polymer chain.[22,27,39,40] This chemistry has been widely used for diverse applications such as anchoring fluorescent dyes,[39] performing stepwise assembly,[27] and manufacturing electrolytes.[40] In the present work, we incorporated the quaternization properties of P2VP into the MPN assembly to expand and investigate the versatility of the assembly. The degree of quaternization of P2VP using methyl iodide at 70 °C at different time points was determined by NMR spectroscopy analysis (Figure 3a). The ratios between the aromatic peaks of P2VP (i.e., 8.3 ppm) and QP2VP (i.e., 8.7 ppm) were used to estimate the degree of quaternization. The degree of quaternized P2VP (QP2VP) in the polymer chain gradually increased with reaction time; specifically, the degrees of quaternization of P2VP were determined to be 3 and 24% for reaction times of 1 and 8 h, respectively. We hypothesized that quaternization could provide additional functionality to the MPN assembly. The quaternization of P2VP occurred concurrently with MPN assembly in the presence of metal ions (e.g., Fe^{III}, Cr^{III}, or Co^{II}). This simultaneous quaternization/MPN assembly produced positively charged capsules (denoted here as QP2VP/P2VP–metal MPN capsules). Control over the surface charge and shell thickness of the MPN capsules were realized by varying the assembly conditions (i.e., temperature and time) (Figure 3a). As the assembly time was prolonged, capsules with thicker shells and a higher degree of positive charges were obtained. P2VP–Fe^{III} MPN capsules, prepared by the conventional MPN assembly process (i.e., t = 0 h), were slightly negatively charged (i.e., −6 ± 2 mV) owing to the deprotonation of the catechol groups in the polymer building blocks (Figure 3b).[21] In contrast,

QP2VP/P2VP–metal MPN capsules with ζ-potential values ranging from 6 ± 1 to 53 ± 4 mV were obtained at increasing assembly times, at 70 °C. As presented in Figure 3c, the shell thickness of QP2VP/P2VP–Fe^{III} MPN capsules increased from ~10 to ~50 nm as the assembly time increased from 1 to 8 h. Control over the shell thickness is attributed to the continuous MPN assembly, which is enabled by coupling MPN assembly with the quaternization of P2VP.

Continuous MPN assembly for engineering the shell thickness of capsules has been previously achieved through an oxidation-mediated process using Fe^{II} precursors[38] and a solid-state reactant-derived assembly using rusted iron objects.[41] Although these processes are well-defined methods to control the shell thickness, the selection of metal ions is restricted to those suitable for these assembly methods. Alternatively, herein, we demonstrate two distinct continuous MPN assembly strategies—P2VP–metal MPN assembly and QP2VP/P2VP–metal MPN assembly—that can be applied to diverse metal ion species (Figure 3d). The assembly mechanisms proposed herein include the participation of molecular interactions (i.e., metal–pyridine or ionic) in addition to discrete metal–coordination networks, which facilitate the continuous assembly process. At the start of both assembly strategies, the biscatechol-P2VP chains approach the template surface, then metal coordination between the catechol groups and metal ions occurs owing to rapid film growth (<1 min).[8,16,38,42,43] The exposed pyridinyl nitrogen atoms on the surface of the layered P2VP–metal MPN films on the templates enable interactions with the polymer building blocks metal ions in the assembly solution. As the reaction progresses, in the P2VP–metal MPN assembly, continuous film growth likely proceeds from coordination interactions between the metal ions and pyridinyl nitrogen atoms in the polymer blocks. In contrast, in the QP2VP/P2VP–metal MPN assembly, quaternization reaction enables continuous assembly by forming ionic interactions between QP2VP rings (positive charges) and deprotonated catechol groups (negative charges).

The quaternized polymers on the surface of capsules and in the assembly solution interact with each other and coordinate with metal ions, which facilitate continuous film formation. Continuous film growth occurring in the QP2VP/P2VP–metal MPN assembly is faster than that occurring in the P2VP–metal MPN assembly. For instance, relative to the shell thickness of QP2VP/P2VP–Fe^{III} MPN capsules obtained at an assembly time of 0 h, that obtained at an assembly time of 8 h assembly increased by 324%, whereas that of P2VP–Fe^{III} MPN capsules only increased by 18% (Figures 3c and S9b). The reaction temperature of the quaternization/MPN assembly also influenced the surface charge and shell thickness of QP2VP/P2VP–Fe^{III} MPN capsules for a given assembly time (Figures 3e, S11–S13). Specifically, the ζ-potential values of the capsules prepared at moderate temperature (i.e., 50 °C) slowly increased compared with capsules prepared at 60 °C and 70 °C. This slower surface charge increase is attributed to the lower rate of quaternization with decreasing quaternization temperature.[44] Likewise, the QP2VP/P2VP–Fe^{III} MPN capsules obtained at 50 and 60 °C were less thick, owing to the relatively slower quaternization process compared with that occurring at 70 °C. The quaternization/MPN assembly was also applicable to different metal ion species, such as Cr^{III} and Co^{II}, indicating the versatility of this assembly method for controlling surface charge and shell thickness. These results indicate that combining MPN assembly with quaternization represents a versatile strategy for engineering the physicochemical properties of MPN capsules.

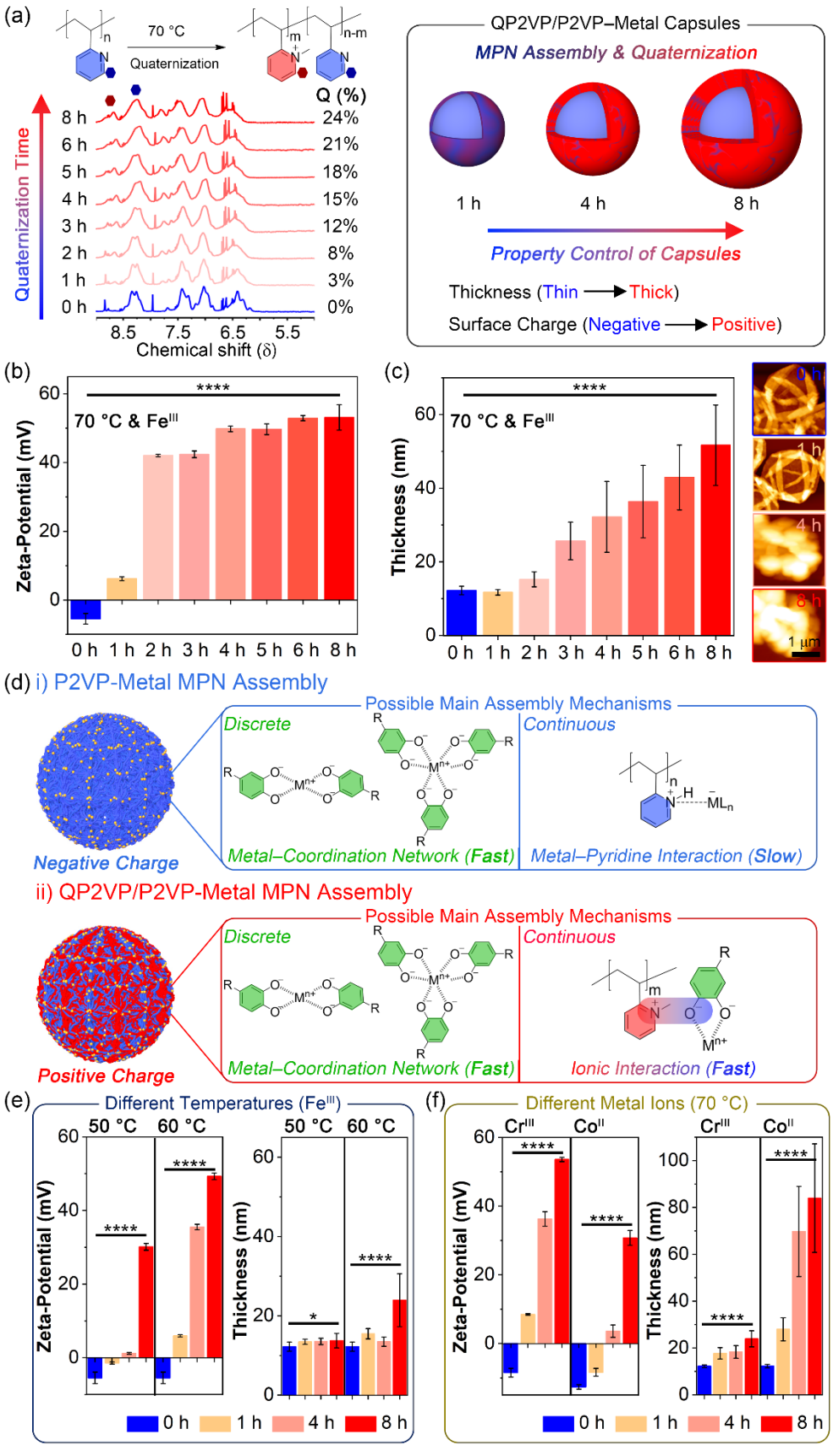
(a)
70 °C
Quaternization
n-m
Q (%)
Quaternization Time
8 h 24%
6 h 21%
5 h 18%
4 h 15%
3 h 12%
2 h 8%
1 h 3%
0 h 0%
8.5 7.5 6.5 5.5
Chemical shift (δ)
QP2VP/P2VP–Metal Capsules
MPN Assembly & Quaternization
1 h
4 h
8 h
Property Control of Capsules
Thickness (Thin → Thick)
Surface Charge (Negative → Positive)
(b)
70 °C & Fe^III
Zeta-Potential (mV)
0 h 1 h 2 h 3 h 4 h 5 h 6 h 8 h
(c)
70 °C & Fe^III
Thickness (nm)
0 h 1 h 2 h 3 h 4 h 5 h 6 h 8 h
1 μm
(d) i) P2VP-Metal MPN Assembly
Negative Charge
Possible Main Assembly Mechanisms
Discrete
Continuous
Metal–Coordination Network (Fast)
Metal–Pyridine Interaction (Slow)
ii) QP2VP/P2VP-Metal MPN Assembly
Positive Charge
Possible Main Assembly Mechanisms
Discrete
Continuous
Metal–Coordination Network (Fast)
Ionic Interaction (Fast)
(e)
Different Temperatures (Fe^III)
50 °C 60 °C
Zeta-Potential (mV)
Thickness (nm)
0 h 1 h 4 h 8 h
(f)
Different Metal Ions (70 °C)
Cr^III Co^II
Zeta-Potential (mV)
Thickness (nm)
0 h 1 h 4 h 8 h

Figure 3. (a) NMR spectra of $QP2VP_m/P2VP_{76-m}$ for determining the degree of quaternization of $P2VP_{76}$ by methyl iodide as a function of reaction time. Schematic illustration of QP2VP/P2VP–metal MPN capsules (prepared by concurrent quaternization/MPN assembly) featuring controllable physicochemical properties according to the reaction time (i.e., degree of quaternization). (b) ζ-Potential and (c) shell thickness of $QP2VP_m/P2VP_{76-m}$–Fe^{III} MPN capsules prepared using different quaternization/MPN assembly times at 70 °C. Inset in (c) shows the corresponding AFM images of capsules obtained after 0, 1, 4, and 8 h. (d) Proposed mechanisms of the P2VP–metal MPN assembly (i.e., metal–coordination network and metal–pyridine interaction) (i) and QP2VP/P2VP–metal MPN assembly (i.e., metal–coordination network and ionic interaction) (ii). ζ-Potential and shell thickness of QP2VP/P2VP–metal MPN capsules prepared using (e) different quaternization/MPN assembly temperatures and (f) different metal ions as a function of assembly time at 70 °C. ζ-Potential data are shown as the mean ± standard deviation of three independent measurements and the shell thickness data (height–distance AFM analysis) are shown as the mean ± standard deviation of 10 independent AFM measurements. Statistical significance was determined by one-way ANOVA: **** $p < 0.0001$ and * $p < 0.05$.

Modularity of Positively Charged MPN Capsules. The positively charged MPN capsules could incorporate negatively charged functional molecules (e.g., dyes and catalytic proteins) through ionic interactions, which would be potentially useful in materials science and biomedical applications such as catalysis, bioimaging, and therapeutic delivery. Six types of QP2VP/P2VP–Fe^{III} MPN capsules were prepared using different temperatures and quaternization/assembly times (i.e., 60 °C, 70 °C, and 4, 6, 8 h) to assess their loading efficiency and post-assembly functionality.

To prepare bioactive and fluorescent capsules, QP2VP/P2VP–Fe^{III} MPN capsules were incubated with HRP and 2000 kDa FITC-dextran in water, respectively (Figure 4a). The HRP

loading was estimated by UV–vis spectrophotometry by comparing the absorbances of the protein solution before loading and the supernatant after loading (Figure S14).[28] The activity of the loaded HRP in the capsules was then examined through the enzymatic oxidation of amplex red to resorufin, which has a strong absorbance at 560 nm, in the presence of H_2O_2.[45] The catalytic rate of the QP2VP/P2VP–Fe^{III} MPN capsules was influenced by the shell properties. Capsules with a higher degree of positive surface charges and thicker films, obtained using higher assembly temperatures and longer assembly times, showed lower catalytic activities, likely due to the strong ionic interaction and steric hindrance from the capsule shell (Figure S15). Therefore, among the capsules examined, the HRP-loaded QP2VP/P2VP–Fe^{III} MPN capsules prepared at 60 °C and assembly time of 4 h showed the highest catalytic activity among prepared HRP-loaded capsules. These capsules showed a 75% conversion compared to that of free HRP at 30 min (Figure 4b). The loading of FITC-dextran into the six types of QP2VP/P2VP–Fe^{III} MPN capsules was investigated through ζ-potential measurements and confocal laser scanning microscopy (CLSM) (Figure 4c). The surface charges of the QP2VP/P2VP–Fe^{III} MPN capsules decreased after loading negatively charged FITC-dextran molecules into the capsules prepared using different temperatures and assembly times from 36 to 3 mV (60 °C–4 h), 49 to 7 mV (60 °C–6 h), 49 to 22 mV (60 °C–8 h), 50 to 13 mV (70 °C–4 h), 53 to 23 mV (70 °C–6 h), and 53 to 25 mV (70 °C–8 h). QP2VP/P2VP–Fe^{III} MPN capsules with a higher degree of positive surface charges and thicker shells (e.g., 70 °C–8 h) displayed brighter fluorescence after incubation with FITC-dextran. These enhanced fluorescence intensities were attributed to the presence of more cationic polymer chains in the capsule shells. In addition, a higher concentration of fluorescent molecules in the incubation solution resulted in a higher FITC loading of the capsules (Figure S16). *Z*-stack images of FITC-dextran-loaded QP2VP/P2VP–Fe^{III} MPN capsules prepared at 70 °C and an assembly time of 8 h

revealed the three-dimensional structure of the fluorescent capsules that featured a uniform distribution of dye molecules on the capsule surface (Figure 4c).

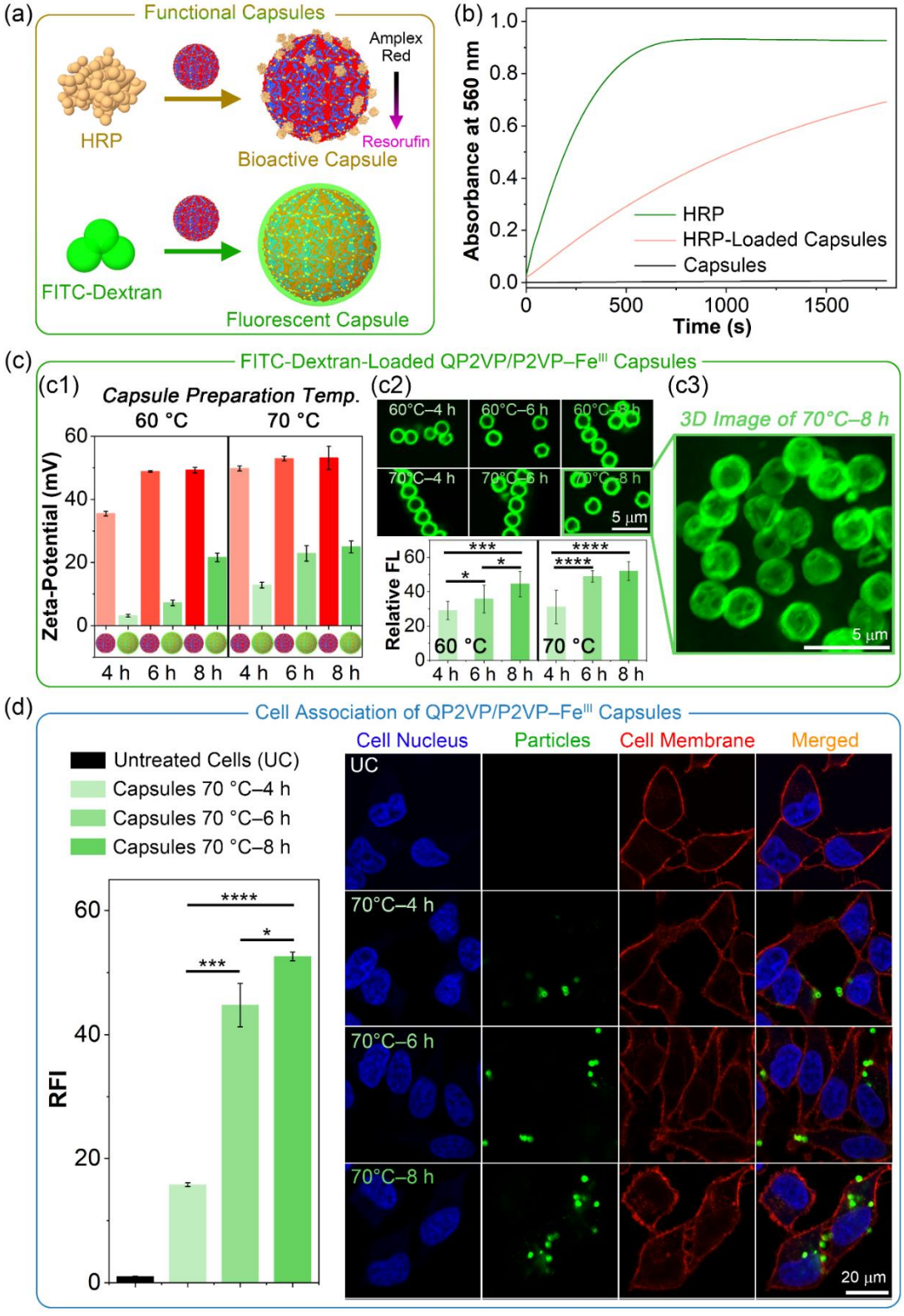

Figure 4. (a) Schematic illustration of the loading of HRP (negatively charged) or FITC-dextran (negatively charged) into QP2VP/P2VP–Fe^{III} MPN capsules (positively charged) through ionic interactions. (b) Time-course plots of the absorbance of amplex red oxidized by free HRP, capsules, and HRP-loaded capsules. (c) Preparation of FITC-dextran-loaded QP2VP/P2VP–Fe^{III} MPN capsules using various QP2VP/P2VP–Fe^{III} MPN capsules prepared using different assembly temperatures and quaternization/MPN assembly reaction times (i.e., 60 °C–4, 6, 8 h and 70 °C–4, 6, 8 h). Comparison of the ζ-potential QP2VP/P2VP–Fe^{III} MPN capsules (red) and FITC-dextran-loaded QP2VP/P2VP–Fe^{III} MPN capsules (green) (c1). CLSM images of FITC-dextran loading in different QP2VP/P2VP–Fe^{III} MPN capsules and relative fluorescence quantification (c2). Three-dimensional image of fluorescent FITC-dextran-loaded QP2VP/P2VP–Fe^{III} MPN capsules (70 °C–8 h) created by merging *z*-section CLSM images (c3). (d) Association of HeLa cells with different QP2VP/P2VP–Fe^{III} MPN capsules, following incubation for 24 h at 37 °C at a cell-to-particle ratio of 1:10. RFI to untreated cells is shown. Error bars represent the standard deviation of three independent experiments. Statistical significance was determined by one-way ANOVA: **** $p < 0.0001$, *** $p < 0.001$, and * $p < 0.05$. CLSM images of HeLa cells incubated with fluorescent capsules for 24 h at 37 °C. Cell membranes and nuclei were stained with wheat germ agglutinin 594 (red) and Hoechst 33342 (blue), respectively. Green fluorescence represents the capsules.

Surface charge is known to be a key parameter that controls the bio–nano interactions of particles, including cell association, pharmacokinetics, and drug loading/release profiles.[1,46] We thus evaluated how the different surface charges of the green-fluorescent QP2VP/P2VP–Fe^{III} MPN capsules would influence cell association. Flow cytometry and CLSM were used to investigate the cell association properties of fluorescent QP2VP/P2VP–Fe^{III} MPN capsules (Figure 4d and S17).

The degree of cell association of fluorescent QP2VP/P2VP–Fe^{III} MPN capsules prepared at 70 °C and quaternization/assembly times of 4, 6, and 8 h was compared using relative fluorescence intensity (RFI) values compared to untreated cells. As shown in Figure 4d, capsules with a higher degree of positive charges showed more significant cell association. Specifically, the RFI values of fluorescent QP2VP/P2VP–Fe^{III} MPN capsules prepared at 70 °C and quaternization/assembly times of 4, 6, and 8 h, following 24 h incubation and using a cell-to-particle ratio 1:10, were determined to be 15.8, 44.8, and 52.6, respectively. To circumvent overlap with green fluorescence from the capsules, Hoechst 33342 (blue) and wheat germ agglutinin 594 (red) were used to stain the cell nucleus and membrane. Consistent with the flow cytometry measurements, CLSM analysis showed that QP2VP/P2VP–Fe^{III} MPN capsules prepared at 70 °C and using a quaternization/assembly time of 8 h (which are the most positively charged) showed the highest cell association (Figure 4d) among the capsules prepared with different assembly times. The same increasing trend in cell association as assembly time increased was observed for capsules prepared at 60 °C (Figure S17). Cell association of all fluorescent QP2VP/P2VP–Fe^{III} MPN capsules could also be increased by prolonging the incubation time (i.e., from 2 to 4, 8, and 24 h), as investigated by flow cytometry (Figure S17a, b).

The QP2VP/P2VP–Fe^{III} MPN capsules prepared at different assembly temperatures (i.e., 50, 60, and 70 °C) generally showed negligible cytotoxicity (Figure S18) except for the QP2VP/P2VP–Fe^{III} MPN capsules prepared at 70 °C and assembly times of 6 and 8 h. These capsules showed some cytotoxicity to cells when the particle-to-cell ratio increased to 100:1, likely due to the toxicity induced by the higher degree of positive charges.[47] These results indicate that simultaneous quaternization/MPN assembly using P2VP building blocks is a versatile method for

fabricating biofunctional and fluorescent materials that are potentially useful for biomedical applications.

CONCLUSIONS

Conventional MPN systems mostly result in negatively charged assemblies, which is based on the exclusive negative charge of phenolic building blocks and metal–phenolic complexation. In this work, we demonstrated the application biscatechol-terminated P2VP in fabricating P2VP–Fe^{III} MPN capsules that displayed a range of surface charge from negative to positive depending on the pH of the dispersant/solution. In addition, we exploited the capsules as building blocks for the preparation of secondary hollow superstructures. Our strategy enabled continuous MPN film growth, likely due to the coordination networks between pyridinyl nitrogen atoms in the building blocks and the metal ions, and was applicable to a range of metal ions (i.e., Al^{III}, V^{III}, Cr^{III}, Fe^{III}, and Co^{II}). In addition, quaternizing the P2VP chains in tandem with MPN assembly provided a pathway to fabricate positively charged MPN capsules (i.e., QP2VP/P2VP–metal MPN capsules) with controllable surface charge and shell thickness. The capsule properties were influenced by the preparation conditions (e.g., assembly temperature, reaction time, and metal ion species). Bioactive and fluorescent capsules were obtained through ionic interactions between the cationic capsules and anionic functional molecules (i.e., HRP and FITC-dextran), and the cell association properties of the capsules were controlled via the surface charge of the capsules. Capsules with a higher degree of positive charges resulted in greater cell association. This study provides insights into the application of versatile building blocks in MPN assembly and expands the toolbox of MPN building blocks. In addition, this study can provide a strategy for optimizing metal–organic particle systems for therapeutic nucleic acid delivery (i.e., mRNA and siRNA)[48] by regulating the loading efficiency through tuning the charge of building blocks.

ASSOCIATED CONTENT

Supporting Information. Materials and instrumentation; synthesis protocols for BDAT, biscarboxylic acid-functionalized P2VP, biscatechol-functionalized P2VP, AuNPs, and hollow superstructures; procedures for structural stability investigation of MPN capsules, permeability studies, HRP activity studies, cell association studies of MPN capsules, and cell viability test; ^{1}H NMR, gel permeation chromatography, and Fourier transform infrared data for synthesized polymers; additional AFM images of P2VP–metal and QP2VP$_m$/P2VP$_{76-m}$–Fe^{III} MPN capsules; additional differential interference contrast images of P2VP$_{76}$–Fe^{III} capsules in various solutions; characterization of AuNPs; detailed permeability comparison of P2VP–metal MPN capsules; additional HRP data of QP2VP/P2VP–Fe^{III} MPN capsules prepared at varying assembly conditions; CLSM images of FITC-dextran-loaded QP2VP/P2VP–Fe^{III} MPN capsules; additional cell association and cytotoxicity data of QP2VP/P2VP–Fe^{III} MPN capsules prepared at varying assembly conditions; and Minimum Information Reporting in Bio-Nano Experimental Literature (MIRIBEL) checklist.

AUTHOR INFORMATION

Corresponding Author

*E-mail: fcaruso@unimelb.edu.au (F.C.)

Notes

The authors declare no competing financial interest.

ACKNOWLEDGMENTS

This research was funded by the Australian Research Council (ARC) through the Discovery Project (DP200100713) scheme. C.-J.K. acknowledges the research grant of the new professor of

the Gyeongsang National University in 2024 (GNU-2024-240040) and “Regional Innovation Strategy (RIS)” through the National Research Foundation of Korea (NRF) funded by the Ministry of Education (MOE) (2021RIS-003). J.F.Q. acknowledges receipt of a Future Fellowship (FT170100144) from the ARC. This work was performed in part at the Materials Characterisation and Fabrication Platform at The University of Melbourne, the Ian Holmes Imaging Centre at the Bio21 Institute, and the Victorian Node of the Australian National Fabrication Facility.

REFERENCES

1. Ju, Y.; Kim, C. J.; Caruso, F. Functional Ligand-Enabled Particle Assembly for Bio–Nano Interactions. *Acc. Chem. Res.* **2023**, *56*, 1826−1837.

2. Shim, T. S.; Estephan, Z. G.; Qian, Z.; Prosser, J. H.; Lee, S. Y.; Chenoweth, D. M.; Lee, D.; Park, S.-J.; Crocker, J. C. Shape Changing Thin Films Powered by DNA Hybridization. *Nat. Nanotechnol.* **2017**, *12*, 41–47.

3. Lu, Y.; Lin, J.; Wang, L.; Zhang, L.; Cai, C. Self-Assembly of Copolymer Micelles: Higher-Level Assembly for Constructing Hierarchical Structure. *Chem. Rev.* **2020**, *120*, 4111−4140.

4. Cai, J.; Manners, I.; Qiu, H. “Self-Adaptive” Coassembly of Colloidal “Saturn-like” Host–Guest Complexes Enabled by Toroidal Micellar Rubber Bands. *J. Am. Chem. Soc.* **2022**, *144*, 5734–5738.

5. Qiu, R.; Sasselli, I. R.; Alvarez, Z.; Sai, H.; Ji, W.; Palmer, L. C.; Stupp, S. I. Supramolecular Copolymers of Peptides and Lipidated Peptides and Their Therapeutic Potential. *J. Am. Chem. Soc.* **2022**, *144*, 5562–5574.

6. Chan, M. H.; Yam, V. W. Toward the Design and Construction of Supramolecular Functional Molecular Materials Based on Metal–Metal Interactions. *J. Am. Chem. Soc.* **2022**, *144*, 22805–22825.

7. Zhou, J.; Lin, Z.; Ju, Y.; Rahim, M. A.; Richardson, J. J.; Caruso, F. Polyphenol-Mediated Assembly for Particle Engineering. *Acc. Chem. Res.* **2020**, *53*, 1269–1278.

8. Kim, C.-J.; Goudeli, E.; Ercole, F.; Ju, Y.; Gu, Y.; Xu, W.; Quinn, J. F.; Caruso, F. Particle Engineering Via Supramolecular Assembly of Macroscopic Hydrophobic Building Blocks. *Angew. Chem. Int. Ed.* **2024**, *63*, e202315297.

9. Kim, C.-J.; Ercole, F.; Chen, J.; Pan, S.; Ju, Y.; Quinn, J. F.; Caruso, F. Macromolecular Engineering of Thermoresponsive Metal–Phenolic Networks. *J. Am. Chem. Soc.* **2022**, *144*, 503–514.

10. Chen, J.; Cortez-Jugo, C.; Kim, C.-J.; Lin, Z.; Wang, T.; De Rose, R.; Xu, W.; Wang, Z.; Gu, Y.; Caruso, F. Metal–Phenolic-Mediated Assembly of Functional Small Molecules into Nanoparticles: Assembly and Bioapplications. *Angew. Chem. Int. Ed.* **2024**, *63*, e202319583.

11. Qu, Y.; De Rose, R.; Kim, C.-J.; Zhou, J.; Lin, Z.; Ju, Y.; Bhangu, S. K.; Cortez-Jugo, C.; Cavalieri, F.; Caruso, F. Supramolecular Polyphenol–DNA Microparticles for In Vivo Adjuvant and Antigen Co-Delivery and Immune Stimulation. *Angew. Chem. Int. Ed.* **2023**, *62*, e202214935.

12. Jiang, L.; Zeng, Y.; Li, H.; Lin, Z.; Liu, H.; Richardson, J. J.; Gao, Z.; Wu, D.; Liu, L.; Caruso, F. Peptide-Based Coacervate Protocells with Cytoprotective Metal–Phenolic Network Membranes. *J. Am. Chem. Soc.* **2023**, *145*, 24108–24115.

13. Wang, Q.; Gao, Z.; Zhong, Q.-Z.; Wang, N.; Mei, H.; Dai, Q.; Cui, J.; Hao, J. J. L. Encapsulation of Enzymes in Metal–Phenolic Network Capsules for the Trigger of Intracellular Cascade Reactions. *Langmuir* **2021**, *37*, 11292−11300.

14. Rizzuto, F. J.; Platnich, C. M.; Luo, X.; Shen, Y.; Dore, M. D.; Lachance-Brais, C.; Guarné, A.; Cosa, G.; Sleiman, H. F. A Dissipative Pathway for the Structural Evolution of DNA Fibres. *Nat. Chem.* **2021**, *13*, 843–849.

15. Choi, G.; Fitriasari, E. I.; Park, C. Electro-Mechanochemical Gating of a Metal–Phenolic Nanocage for Controlled Guest-Release Self-Powered Patches and Injectable Gels. *ACS Nano* **2021**, *15*, 14580–14586.

16. Ejima, H.; Richardson, J. J.; Liang, K.; Best, J. P.; van Koeverden, M. P.; Such, G. K.; Cui, J.; Caruso, F. One-Step Assembly of Coordination Complexes for Versatile Film and Particle Engineering. *Science* **2013**, *341*, 154–157.

17. Kim, C.-J.; Ercole, F.; Ju, Y.; Pan, S.; Chen, J.; Qu, Y.; Quinn, J. F.; Caruso, F. Synthesis of Customizable Macromolecular Conjugates as Building Blocks for Engineering Metal–Phenolic Network Capsules with Tailorable Properties. *Chem. Mater.* **2021**, *33*, 8477–8488.

18. Chen, J.; Pan, S.; Zhou, J.; Zhong, Q.-Z.; Qu, Y.; Richardson, J. J.; Caruso, F. Programmable Permeability of Metal–Phenolic Network Microcapsules. *Chem. Mater.* **2020**, *32*, 6975−6982.

19. Xu, W.; Pan, S.; Noble, B. B.; Lin, Z.; Bhangu, S. K.; Kim, C.-J.; Chen, J.; Han, Y.; Yarovsky, I.; Caruso, F. Engineering Flexible Metal–Phenolic Networks with Guest Responsiveness Via Intermolecular Interactions. *Angew. Chem. Int. Ed.* **2023**, *62*, e202302448.

20. Kim, C.-J.; Ercole, F.; Goudeli, E.; Bhangu, S. K.; Chen, J.; Faria, M.; Quinn, J. F.; Caruso, F. Engineering Programmable DNA Particles and Capsules Using Catechol-Functionalized DNA Block Copolymers. *Chem. Mater.* **2022**, *34*, 7468–7480.

21. Bijlsma, J.; de Bruijn, W. J. C.; Hageman, J. A.; Goos, P.; Velikov, K. P.; Vincken, J. P. Revealing the Main Factors and Two-Way Interactions Contributing to Food Discolouration Caused by Iron-Catechol Complexation. *Sci. Rep.* **2020**, *10*, 8288.

22. Kennemur, J. G. Poly(vinylpyridine) Segments in Block Copolymers: Synthesis, Self-Assembly, and Versatility. *Macromolecules* **2019**, *52*, 1354–1370.

23. Lee, D.; Kim, J.; Ku, K. H.; Li, S.; Shin, J. J.; Kim, B. J. Poly(vinylpyridine)-Containing Block Copolymers for Smart, Multicompartment Particles. *Polym. Chem.* **2022**, *13*, 2570–2588.

24. Anslyn, E. V.; Dougherty, D. A. *Modern Physical Organic Chemistry*; University Science Books: Sausalito, California, 2006.

25. Balazs, A. C.; Emrick, T.; Russell, T. P. Nanoparticle Polymer Composites: Where Two Small Worlds Meet. *Science* **2006**, *314*, 1107–1110.

26. Fréchet, J. M.; de Meftahi, M. V. Poly(vinyl pyridine)s: Simple Reactive Polymers with Multiple Applications. *Br. Polym. J.* **1984**, *16*, 193–198.

27. Hanisch, A.; Gröschel, A. H.; Förtsch, M.; Drechsler, M.; Jinnai, H.; Ruhland, T. M.; Schacher, F. H.; Müller, A. H. Counterion-Mediated Hierarchical Self-Assembly of an ABC Miktoarm Star Terpolymer. *ACS Nano* **2013**, *7*, 4030–4041.

28. Lin, Z.; Zhou, J.; Cortez-Jugo, C.; Han, Y.; Ma, Y.; Pan, S.; Hanssen, E.; Richardson, J. J.; Caruso, F. Ordered Mesoporous Metal–Phenolic Network Particles. *J. Am. Chem. Soc.* **2020**, *142*, 335–341.

29. Lai, J. T.; Filla, D.; Shea, R. Functional Polymers from Novel Carboxyl-Terminated Trithiocarbonates as Highly Efficient RAFT Agents. *Macromolecules* **2002**, *35*, 6754–6756.

30. Isakova, A.; Topham, P. D.; Sutherland, A. J. Controlled RAFT Polymerization and Zinc Binding Performance of Catechol-Inspired Homopolymers. *Macromolecules* **2014**, *47*, 2561–2568.

31. Schweigert, N.; Zehnder, A. J.; Eggen, R. I. Chemical Properties of Catechols and Their Molecular Modes of Toxic Action in Cells, from Microorganisms to Mammals: Minireview. *Environ. Microbiol.* **2001**, *3*, 81–91.

32. Liu, Y.; Jia, J.; Liu, Z.; Pu, N.; Ye, G.; Wang, W.; Hu, T.; Qi, T.; Chen, J. Competitive Binding-Modulated Metal–Phenolic Assemblies for Adaptable Nanofilm Engineering. *Chem. Mater.* **2021**, *33*, 4733–4744.

33. Geng, H.; Zhong, Q. Z.; Li, J.; Lin, Z.; Cui, J.; Caruso, F.; Hao, J. Metal Ion-Directed Functional Metal–Phenolic Materials. *Chem. Rev.* **2022**, *122*, 11432–11473.

34. Chen, J.; Pan, S.; Zhou, J.; Seidel, R.; Beyer, S.; Lin, Z.; Richardson, J. J.; Caruso, F. Metal–Phenolic Networks as Tunable Buffering Systems. *Chem. Mater.* **2021**, *33*, 2557–2566.

35. Lee, J.; Kwak, J.; Choi, C.; Han, S. H.; Kim, J. K. Phase Behavior of Poly(2-vinylpyridine)-*Block*-Poly(4-vinylpyridine) Copolymers Containing Gold Nanoparticles. *Macromolecules* **2017**, *50*, 9373–9379.

36. Turkevich, J.; Stevenson, P. C.; Hillier, J. A Study of the Nucleation and Growth Processes in the Synthesis of Colloidal Gold. *Discuss. Faraday Soc.* **1951**, *11*, 55–75.

37. Rahim, A. M.; Kempe, K.; Mullner, M.; Ejima, H.; Ju, Y.; van Koeverden, M. P.; Suma, T.; Braunger, J. A.; Leeming, M. G.; Abrahams, B. F.; Caruso, F. Surface-Confined Amorphous Films from Metal-Coordinated Simple Phenolic Ligands. *Chem. Mater.* **2015**, *27*, 5825–5832.

38. Zhong, Q.-Z.; Li, S.; Chen, J.; Xie, K.; Pan, S.; Richardson, J. J.; Caruso, F. Oxidation-Mediated Kinetic Strategies for Engineering Metal–Phenolic Networks. *Angew. Chem. Int. Ed.* **2019**, *58*, 12563–12568.

39. Cai, J.; Li, C.; Kong, N.; Lu, Y.; Lin, G.; Wang, X.; Yao, Y.; Manners, I.; Qiu, H. Tailored Multifunctional Micellar Brushes Via Crystallization-Driven Growth from a Surface. *Science* **2019**, *366*, 1095–1098.

40. Arges, C. G.; Kambe, Y.; Dolejsi, M.; Wu, G.-P.; Segal-Pertz, T.; Ren, J.; Cao, C.; Craig, G. S.; Nealey, P. F. Interconnected Ionic Domains Enhance Conductivity in Microphase Separated Block Copolymer Electrolytes. *J. Mater. Chem. A* **2017**, *5*, 5619–5629.

41. Rahim, A. M.; Bjoernmalm, M.; Bertleff-Zieschang, N.; Besford, Q.; Mettu, S.; Suma, T.; Faria, M.; Caruso, F. Rust-Mediated Continuous Assembly of Metal–Phenolic Networks. *Adv. Mater.* **2017**, *29*, 1606717.

42. Guo, J.; Tardy, B. L.; Christofferson, A. J.; Dai, Y.; Richardson, J. J.; Zhu, W.; Hu, M.; Ju, Y.; Cui, J.; Dagastine, R. R.; Yarovsky, I.; Caruso, F. Modular Assembly of Superstructures from Polyphenol-Functionalized Building Blocks. *Nat. Nanotechnol.* **2016**, *11*, 1105–1111.

43. Bhangu, S. K.; Charchar, P.; Noble, B. B.; Kim, C.-J.; Pan, S.; Yarovsky, I.; Cavalieri, F.; Caruso, F. Origins of Structural Elasticity in Metal–Phenolic Networks Probed by Super-Resolution Microscopy and Multiscale Simulations. *ACS Nano* **2022**, *16*, 98–110.

44. De Jesús-Téllez, M. A.; Sánchez-Cerrillo, D. M.; Quintana-Owen, P.; Schubert, U. S.; Contreras-López, D.; Guerrero-Sánchez, C. Kinetic Investigations of Quaternization Reactions of Poly[2-(dimethylamino)ethyl Methacrylate] with Diverse Alkyl Halides. *Macromol. Chem. Phys.* **2020**, *221*, 1900543.

45. Veitch, N. C. Horseradish Peroxidase: A Modern View of a Classic Enzyme. *Phytochemistry* **2004**, *65*, 249–259.

46. Glass, J. J.; Chen, L.; Alcantara, S.; Crampin, E. J.; Thurecht, K. J.; De Rose, R.; Kent, S. J. Charge Has a Marked Influence on Hyperbranched Polymer Nanoparticle Association in Whole Human Blood. *ACS Macro Lett.* **2017**, *6*, 586–592.

47. Yang, W.; Mixich, L.; Boonstra, E.; Cabral, H. Polymer-Based mRNA Delivery Strategies for Advanced Therapies. *Adv. Healthcare Mater.* **2023**, *12*, e2202688.

48. Gu, Y.; Chen, J.; Wang, Z.; Liu, C.; Wang, T.; Kim, C.-J.; Durikova, H.; Fernandes, S.; Johnson, D. N.; De Rose, R. mRNA Delivery Enabled by Metal–Organic Nanoparticles. *Nat. Commun.* **2024**, *15*, 9664.

Table of Content Graphic